The Oklahoma Geological Survey Statewide Seismic Network

by Jacob I. Walter, Paul Ogwari, Andrew Thiel, Fernando Ferrer, Isaac Woelfel, Jefferson C. Chang, Amberlee P. Darold, and Austin A. Holland

ABSTRACT

The Oklahoma Geological Survey (OGS) monitors seismicity throughout the state of Oklahoma utilizing permanent and temporary seismometers installed by OGS and other agencies, while producing a real-time earthquake catalog. The OGS seismic network was recently added to the Advanced National Seismic System (ANSS) as a self-supporting regional seismic network, and earthquake locations and magnitudes are automatically reported through U.S. Geological Survey and are part of the ANSS Comprehensive Earthquake Catalog. In Oklahoma, before 2009, background seismicity rates were about 2 **M** 3.0 + earthquakes per year, which increased to 579 and 903 **M** 3.0+ earthquakes in 2014 and 2015, respectively. After seismicity peaked, the rate fell to 624, 304, and 194 **M** 3.0+ earthquakes in 2016, 2017, and 2018, respectively. The catalog is complete down to **M** 2.2 from mid-2014 to present, despite the significant workload for a primarily state-funded regional network. That astonishing uptick in seismicity has been largely attributed to wastewater injection practices. The OGS provides the Oklahoma Corporation Commission, the agency responsible for regulating oil and gas activities within the state, with technical guidance and earthquake products that inform their "traffic-light" mitigation protocol and other mitigating actions. We have initiated a citizen-scientist-driven, educational seismometer program by installing Raspberry Shake geophones throughout the state at local schools, museums, libraries, and state parks. The seismic hazard of the state portends a continued need for expansion and densification of seismic monitoring throughout Oklahoma.

Supplemental Material

BACKGROUND

Geology and Historical Earthquakes

The underlying geology of Oklahoma can be characterized by marine sedimentation with brief periods of uplift and subsidence. The long period of subsidence created deep sedimentary units that contribute to Oklahoma being a vast resource of hydrocarbon source rocks and deposits (Lawson and Luza, 1995). Those periods of subsidence were terminated by protracted periods of uplift, which brought granite to the surface in southern Oklahoma and formed the tectonic zone known as the Amarillo-Wichita uplift. That tectonic feature, which includes uplifted granite, extends west-northwest from south-central Oklahoma into the Texas Panhandle, and forms a belt of seismicity active in the present (Walter *et al.*, 2018). In central and northern Oklahoma, the subsurface geology consists of fractured intrusives and crystalline basement (Shah and Keller, 2017) overlain by the sediments from the aforementioned periods of subsidence and marine sedimentation.

Oklahoma is riddled with structural features comprising steeply dipping north–south fault systems that separate geologic provinces (e.g., Northcutt and Campbell, 1995). The structural features include zones that act as traps for hydrocarbons, and thus, considerable effort has gone into mapping the geology in these areas. The Nemaha fault system, one such north–south feature, that crosses central Oklahoma formed from a tectonic event in the Mississippian and consists of uplifted blocks 5–8 km wide bounded by faults on either side (Lawson and Luza, 1995). East of the Nemaha uplift there are a series of several grabens separated by (from west to east) the Wilzetta, Keokuk, Wewoka, Weleetka, and East Mountain fault zones (Dycus, 2013; Dudek, 2014). These named faults, although easily identified through well log analysis, include subtle surface expressions of small antithetical faults along their respective main traces.

In southern Oklahoma, the Meers fault is a large fault that is plausibly capable of rupturing in an **M** 7.0+ earthquake. The most recent evidence of rupture has been dated to as recently as ~1300 yr ago (Crone and Luza, 1990). The fault is one of two faults in North America, east of the Rocky Mountains, with visible surface offset that displaces Holocene sediments and thus possibly represents the largest known earthquake hazard in the central United States. Over the past few decades, Oklahoma Geological Survey (OGS) scientists and other collaborating institutions have engaged in paleoseismological and shallow geophysical surveys to ascertain the seismic sequence history. Trenching and surface mapping suggest that the rupture length would be consistent with at least an **M** 7.0+ event

doi: 10.1785/0220190211

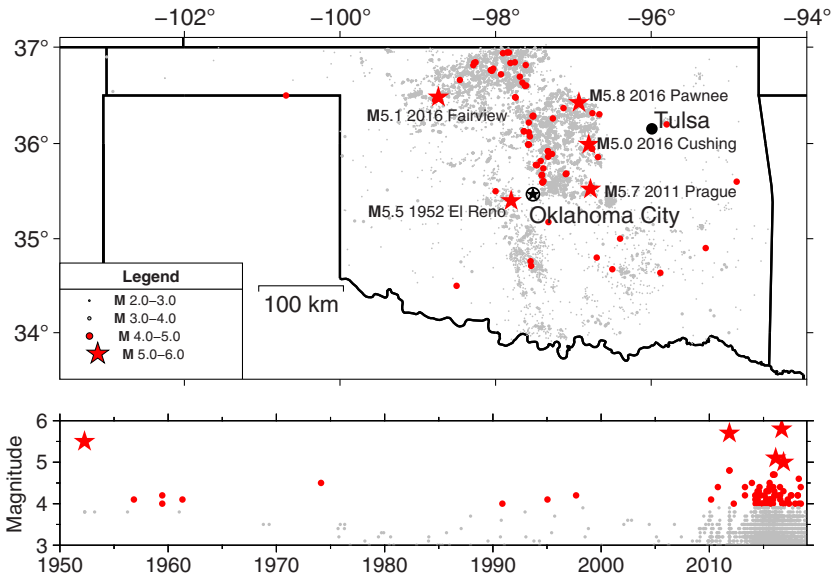

▲ **Figure 1.** Historical earthquakes in Oklahoma from the Oklahoma Geological Survey (OGS) catalog (see Data and Resources) with symbols corresponding to earthquake magnitudes and labels for those earthquakes greater than or equal to **M** 5.0. Note that seismicity from adjacent states is not mapped. The color version of this figure is available only in the electronic edition.

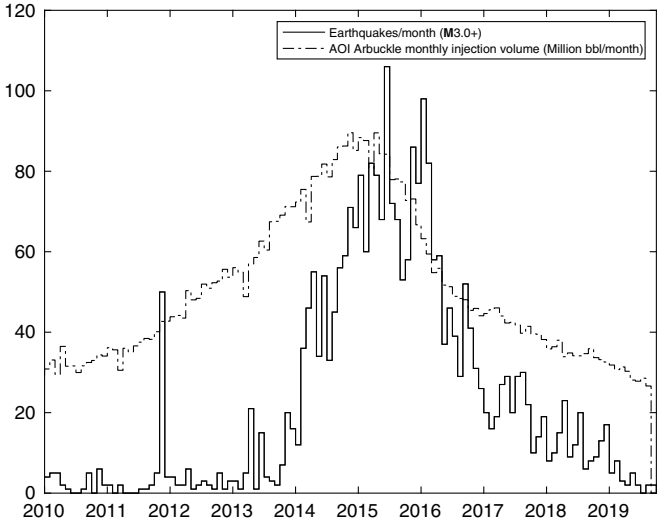

▲ **Figure 2.** Seismicity rate (earthquakes **M** 3.0+ per month) from the OGS catalog (solid line) and Arbuckle Group wastewater disposal monthly volumes (dashed line) within the Oklahoma Corporation Commission area of interest that comprises much of north-central Oklahoma.

(Luza *et al.*, 1987). Preliminary probabilistic seismic hazard analysis (PSHA) from the Meers fault suggests that such an earthquake would cause widespread damage, though additional studies on recurrence interval, rupture lengths, and other variables are needed if PSHAs were conducted for building design guidance or other purposes (Baker and Holland, 2013).

Oklahoma has experienced at least five **M** 5.0+ earthquakes within the written historical record (Table 1). Of those earthquakes, four of the five **M** 5.0+ earthquakes have occurred within the past 8 yr. The large earthquake that occurred outside of the past 8 yr was the 1952 **M** 5.5 El Reno earthquake (Fig. 1) that caused moderate damage in El Reno and Oklahoma City, including toppled chimneys and smokestacks, cracked and loosened bricks on buildings, and broken windows and dishes, including a crack in the State Capitol that was approximately 15 m long. Shaking was reported across Oklahoma, including in Kansas, Arkansas, Iowa, Missouri, Nebraska, and Texas. It reportedly triggered a landslide in eastern Oklahoma (Regmi and Walter, 2019). Based on the presence of a few wastewater injection wells within the same county as the event and the nature of the macroseismic reported intensities from newspapers and other archives, Hough and Page (2015) suggested that the El Reno earthquake was possibly induced. They based this suggestion on the spatial proximity of wells, and the limited historical macroseismic observations seem to be consistent with similar observations from more modern measurements of induced earthquakes. However, wastewater injection was common across the state, and the macroseismic signature of induced earthquakes results from the shallowness of the source, as suggested by Hough and Page (2015). Depth is not a particularly diagnostic criterion for determining causation because most Oklahoma earthquakes, both tectonic and induced, are shallow relative to other tectonic zones.

Induced Seismicity

Late in the evening at 10:53 p.m. local time on 5 November 2011, Oklahomans east of Oklahoma City were awakened by what was then the largest earthquake in recorded history. That earthquake, an **M** 5.7 with an epicenter near Prague, was later eclipsed in size by the 3 September 2016 **M** 5.8 earthquake near Pawnee, Oklahoma. The Prague earthquake, which actually occurred on 6 November 2011 03:53 UTC, caused some injuries, and damage was substantial, including famously collapsing a turret and damaging other turrets at St. Gregory's University in Shawnee, Oklahoma. The larger mainshock was preceded by a strong **M** 4.8 foreshock about 20 hr prior. The scientific community largely agrees that the Prague earthquake was probably induced by nearby wastewater injection (Keranen *et al.*, 2013; Sumy *et al.*, 2017). Whereas increased seismicity in central Oklahoma was suspected as being induced by wastewater injection, this earthquake ushered in a wave of scientific studies that more solidly established the relationship.

Subsequent to the Prague earthquake, the seismicity rate continued drastically rising across various regions of Oklahoma (Fig. 2) in what was later understood to be a rise concurrent with an increase in saltwater disposal (Walsh and Zoback, 2015;

Weingarten *et al.*, 2015). Several clusters of previously unmapped faults had significant seismic activity, including areas that culminated in several large earthquakes including the November 2011 M_w 5.7 Prague earthquake (Holland *et al.*, 2012; Keranen *et al.*, 2013), the February 2016 M_w 5.1 Fairview earthquake (Yeck *et al.*, 2016), the September 2016 M_w 5.8 Pawnee earthquake (Chen *et al.*, 2017; Walter *et al.*, 2017; Yeck *et al.*, 2017), and the November 2016 M_w 5.0 Cushing earthquake. During this time period the rate of smaller earthquakes (**M** 3.0+) across the mid-continent of the United States also had dramatically increased, though the increase was especially concentrated in Oklahoma (Ellsworth, 2013). In Oklahoma before 2009, background seismicity rates were about two **M** 3.0+ earthquakes per year, which increased to 579 and 903 **M** 3.0+ earthquakes in 2014 and 2015, respectively.

The increase in seismicity in Oklahoma coincided with development focused around the Mississippian and Hunton Limestones. The target formations include substantial amounts of coproduced formation brines (Murray and Holland, 2014), which required disposal. Oftentimes, the most economic method of disposal included disposal in adjacent injection wells screened through the karst Arbuckle Group and sometimes deeper into the upper basement. From 2010 to late 2014, statewide disposal rates increased from ~30 million bbls per month to ~90 million bbls per month (Fig 2). The increase in seismicity rate roughly corresponded to the increase in monthly injection rates, though sometimes with a lag greater than a year or so in many subregions of Oklahoma (Langenbruch and Zoback, 2016; Goebel *et al.*, 2017). That observation, coupled with the depth of the seismicity occurring mostly within basement rocks and sometimes along previously mapped basement faults, led to the general conclusion that wastewater disposal within the Arbuckle Group was inducing earthquakes across Oklahoma (Walsh and Zoback, 2015).

Since peaks in wastewater injection and seismicity in late 2014 and late 2015, respectively, wastewater injection and seismicity rates have fallen substantially to ~40 million bbls per month and fewer than 10 earthquakes **M** 3.0+ per month. The decrease in injection, which plausibly drives the decrease in seismicity, is in part due to state-mandated reductions in allowable daily disposal rates (Oklahoma Corporation Commission [OCC], 2016a) and oilfield economics; the technical achievements of hydrofracturing and horizontal wells that fueled the domestic midcontinent energy boom contributed to a global oversupply and subsequent industry downturn as the price of oil collapsed during 2014–2015 (Stocker *et al.*, 2018).

Much of the activity in the past 8 yr corresponds to a broad area in north-central Oklahoma where most of the deep wastewater injection disposal occurs into the Arbuckle Group. However, several large events have occurred across southern Oklahoma associated with the aforementioned Amarillo-Wichita uplift in southwest Oklahoma (Walter *et al.*, 2018) and Ouachita thrust belt in southeast Oklahoma, including the 1882 **M** 4.8 Choctaw Nation earthquake (Hough and Page, 2015). The historical earthquake catalog includes small earthquakes (**M** < 4.0) across mapped and unmapped fault structures in Oklahoma, including areas without any hydrocarbon extraction or disposal activities (Fig. 1). Thus, the tectonic seismicity rate across Oklahoma is possibly elevated relative to other regions in the central United States. Because developing hydrocarbons from unconventional shale plays seems to lead to an increase in seismicity (e.g., Ellsworth, 2013), it is perhaps no surprise that industrial activities in the past decade exacerbated the underlying seismic hazard in Oklahoma.

REGIONAL SEISMIC NETWORK

Leonard Facility and Past Regional Studies

The OGS has existed since 1908, having been included in the state's constitution that was ratified in 1907. Whereas some early earthquakes were recorded as having been felt by eyewitness reports, most earthquakes in the state were not instrumentally detected prior to the 1960s (Lawson and Luza, 1995). In 1961, the Jersey Production Research Company installed a seismograph in Leonard, Oklahoma, about 40 km southeast of Tulsa. The seismograph and surrounding land were later donated to the University of Oklahoma, and it was called the Leonard Geophysical Observatory, staffed and administered by the OGS. This seismograph was previously designated with station code TUL, and borehole instrumentation continues to monitor ground motions at the site with station code TUL3 operated by the U.S. Geological Survey (USGS) as part of the N4 network. When installed, TUL was a long-period sensor and not particularly suited to recording local earthquakes for regional monitoring purposes. In 1973, a short-period seismograph was also installed at TUL, though the ability to detect local earthquakes still relied on felt reports with the instrumental record providing further location and magnitude constraints.

In the period between 1977 and 1993, OGS operated a statewide network with radio telemetry for stations near the Leonard facility. Those stations were later converted to digitally transmit their data or digitally record locally. From the period of about 1976–2010 there were about eight permanent seismographs operating in the state. During this time period OGS scientists conducted a regional study on the feasibility for nuclear power facilities, which was funded by the Nuclear Regulatory Commission (Luza and Lawson, 1982), that identified microseismicity across the Nemaha fault zone. In addition, other local studies were supported by various agencies for identifying local earthquakes along specific features, such as near the Meers fault (Luza *et al.*, 1987).

Transportable Array and Early Seismic Network

In the period between 2009 and 2012, Transportable Array (TA) stations as part of the USArray initiative, funded by the National Science Foundation (NSF), were installed at ~70 km spacing throughout the state. Stations were intended to operate for a period of ~2 yr and be utilized for structural seismology studies. Serendipitously for seismologists with interests in induced seismicity, the arrival of TA stations corresponded with the aforementioned rise in earthquake activity associated with the rise in unconventional oil and gas operations across

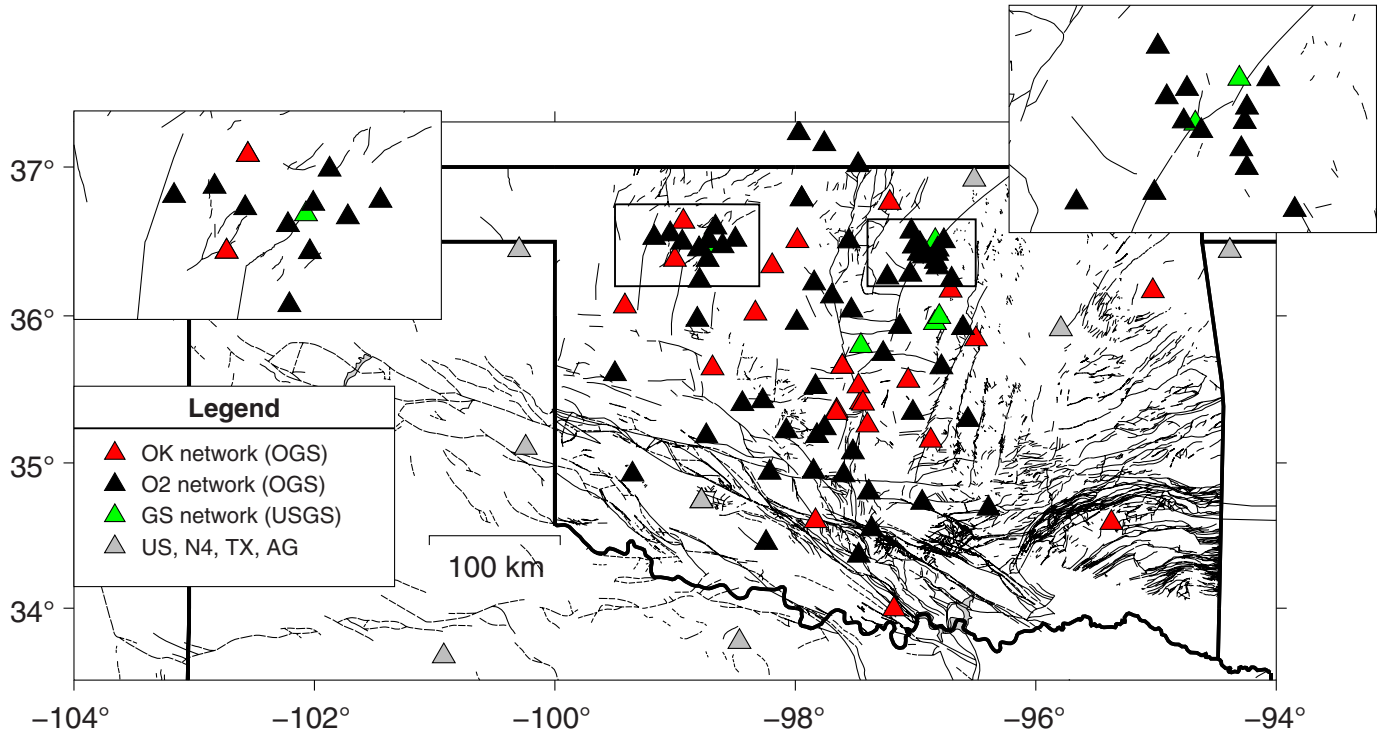

▲ **Figure 3.** Current OGS statewide network configuration, including stations operated by OGS (OK, O2) and stations operated by other agencies that are utilized in real-time earthquake analysis. Oklahoma faults are mapped from Marsh and Holland (2016). A station map with station name labels is included in Ⓔ supplemental material. Top left inset includes stations near Fairview, Oklahoma, and top right inset includes stations near Pawnee, Oklahoma. The inset boundaries are drawn on the main figure. USGS, U.S. Geological Survey. The color version of this figure is available only in the electronic edition.

the mid-continent, and later, in the Appalachian Basin of the eastern United States (e.g., Brudzinski and Kozlowska, 2019). Because much of the NSF investment was incurred during construction of the sites, local agencies were given the opportunity to purchase or "adopt" some permanent stations. During 2011–2012, the OGS adopted and continues maintaining stations U32A, W35A, X34A, and X37A as part of the OK network. The OK network code serves as the permanent station network code for the OGS regional seismic network (RSN).

The adopted TA stations and stations (e.g., station WMOK) operated by other agencies formed the core nucleus of the monitoring stations for the OGS network. In addition, some TA stations continued operating as the N4 network with maintenance handled by Incorporated Research Institutions for Seismology (IRIS) and funded by NSF before being transferred to USGS, including two stations in Oklahoma (T35B and the aforementioned TUL3). Around this time, as funds were made available, several additional stations were added over the next several years, including a subset of stations donated by a local energy company near the Oklahoma City metropolitan area. After large earthquakes, USGS also added several temporary stations across the state, and those stations (network code GS) were incorporated into OGS monitoring. Shortly after the Fairview and Pawnee earthquakes and related swarm activity, the Y9 and Y7 networks, respectively, consisting of temporary stations provided by the Incorporated Research Institutions for Seismology - Portable Array Seismic Studies of the Continental Lithosphere (IRIS-PASSCAL), were installed to capture aftershock activity as part of NSF-funded rapid response programs.

Current Network

In anticipation of hydraulic fracturing across a new unconventional play called the SCOOP/STACK in a region to the west and southwest of Oklahoma City, OGS installed additional IRIS/PASSCAL stations (network code ZP) starting in early 2016. Later, we consolidated all the temporary networks under one network code (O2) in 2018 (Fig. 3). Most of the stations are medium-period or broadband sensors, with just three exceptions where we installed short-period instruments at some OK network stations. Ⓔ Table S1 includes a list of all sensor types with coordinates, and the map in Figure 3 is duplicated with station name labels in the Ⓔ supplemental material (Fig. S1). All OK and O2 stations are streamed in real time on a public seedlink buffer (rtserve.ou.edu port 18000) that the IRIS Data Management Center utilizes for archival and USGS utilizes for detection purposes at the National Earthquake Information Center (NEIC). Metadata for these stations are available through IRIS. Although the O2 and OK networks consist of stations the OGS manages directly, data from the AG, C0,

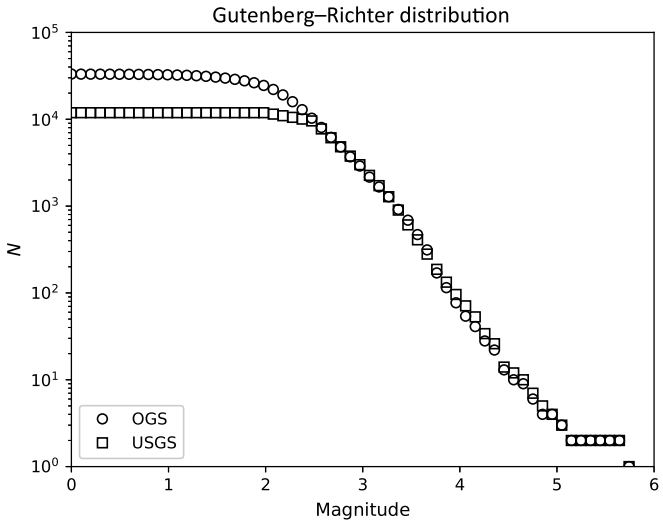

▲ **Figure 4.** Cumulative Gutenberg–Richter style plot of both the USGS (square) and OGS (circle) earthquake catalogs.

GM, GS, N4, TX, and US networks are also accessed through the IRIS real-time seedlink buffer. Because data are streamed in real time and then archived through IRIS, station quality information, including ambient noise levels estimated with power spectral density, is available through the IRIS Mustang data quality webservice (see Data and Resources).

In addition to the professional grade seismometers used in these networks (e.g., Streckeisen STS-2, Güralp CMG-6T, Güralp CMG-3T), Raspberry Shake 1D seismometers have been installed at various locations around the state. We purchased several of these one-component sensors primarily for outreach and education. We have installed them in schools, libraries, museums, and state parks, along with accompanying monitors that show the real-time data and also daylong helicorder plot for the installed stations. Surrounding the monitors, we install explanatory placards describing seismograms, how to locate earthquakes, why wastewater injection induces earthquakes, etc. In addition to the educational role, they may serve to supplement some of the detection capabilities for the primary seismic network (e.g., Anthony *et al.*, 2018). Provisionally, we have tested using these streams for locating earthquakes when coverage by primary stations is lacking, for example, in eastern Oklahoma.

EARTHQUAKE MONITORING

Real-Time Earthquake Location and Magnitude Reporting

Before late 2018, automatic earthquake picking and association was performed using a python-based picker and associator largely built in-house (Chen and Holland, 2016). After events were identified, analysts would refine phase picks, pick polarities, and compute focal mechanisms through the SeisAn software (Havskov and Ottemöller, 1999). Once reviewed, events would populate an OGS database and then be transmitted to USGS through their Product Distribution Layer (PDL). At the time, OGS had no official role within the Advanced National Seismic System (ANSS), and thus USGS analysts at NEIC that received EQXML files would sometimes include earthquake solutions derived from OGS or from NEIC. In other cases, the OGS event location would be used in conjunction with USGS moment tensor analysis for magnitude. Thus, the ANSS Comprehensive Catalog for Oklahoma downloaded at USGS versus OGS (see Data and Resources) may contain several inconsistencies, and these should be noted for hazards analysis or research purposes (Fig. 4). In late 2018, OGS joined ANSS as a self-funded network, and there are tentative plans to resolve some of these historical incongruities between the earthquake catalogs.

Current OGS earthquake monitoring consists of a SeisComP3 (SC3) system capable of detecting, locating, and computing an earthquake magnitude within seconds of an earthquake occurring (Weber *et al.*, 2007). The preliminary localization and magnitude determination is completed even before body waves reach all stations within the state. As time progresses and further data are collected, the automatic locator system modifies the estimated magnitude, depth, and location with the acquisition of additional data. We distribute the SC3 workload across several virtual machines (VMs) within a private cloud managed at the University of Oklahoma (Fig. 5). Data flow comes from network stations to an REF TEK Protocol Daemon (RTPD) server, and a server running acquisition modules connects to that RTPD server as well as outside seedlink connections to either IRIS or individual stations that utilize Q330 dataloggers. A separate VM connects to the SC3 acquisition VM and runs the public seedlink connection. The SC3 processing VM processes the waveform data and produces candidate automatic locations and magnitudes. Core components of SC3 are open source, and we also utilize proprietary modules commercialized by gempa GmbH to improve the reliability of earthquake association.

During regular business hours, manual processing of earthquakes in SC3 is streamlined such that events can be processed within minutes. Because of the lack of resources to staff earthquake monitoring at all hours, we have made several operational decisions related to public publishing of automatic solutions. First, to provide timely earthquake information, we initially post automatic earthquake solutions. We developed a python listener script that runs continually within the SC3 processing VM and determines whether automatically located events should populate the public database that meet certain minimum criteria, such as phase count and association quality. Once these criteria are met, an event is written to a separate PostgreSQL database on a separate VM. Once written to the database, the public is able to view these events by downloading the catalog or viewing the OGS recent earthquakes webpage (see Data and Resources), but are listed as *preliminary*. Once an event is reviewed by an analyst, the event is updated within the PostgreSQL database and the public designation changes to *reviewed*. In cases of larger events (**M** 3.8 or greater) during off-business hours, the processing system is accessed remotely to verify and review events.

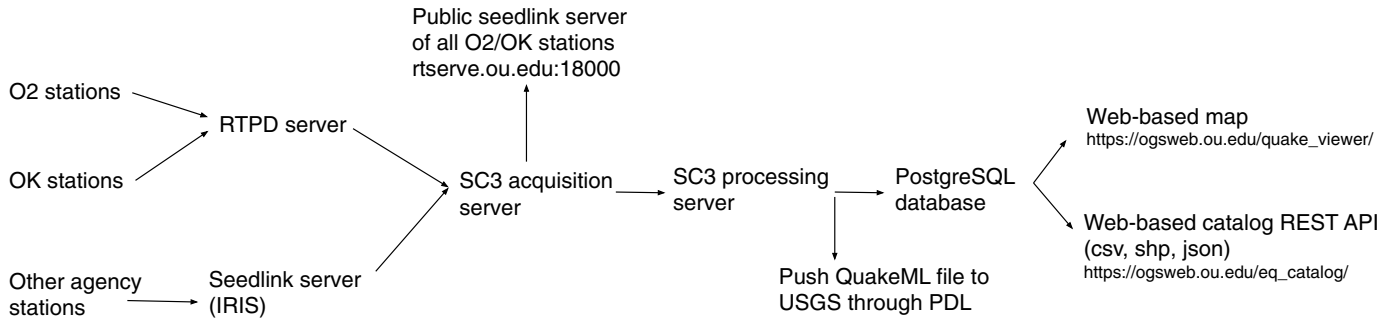

▲ **Figure 5.** Flow diagram of earthquake monitoring system. IRIS, Incorporated Research Institutions for Seismology; REST API, Representational State Transfer Application Program Interface; RTPD, REF TEK Protocol Daemon; Sc3, SeisComP3.

Through our official inclusion in ANSS, earthquake locations and magnitudes are sent to USGS through PDL and are authoritative within Oklahoma. For internal purposes, we still locate and review events within approximately one county in surrounding states as shaking from these earthquakes could plausibly be felt within the state, and we are charged with providing that timely information to Oklahoma citizens. These state-adjacent events are not forwarded through PDL but available through OGS web applications.

Although we have tuned our local magnitude (M_L) calculation so that estimates of local magnitude should be equivalent to USGS moment magnitude (M_w) estimates, for larger events we defer to the moment magnitude calculated at NEIC because they are using a waveform-based approach to estimate M_w. It is widely accepted in the community that a waveform-based approach is preferred relative to a Richter-like approach that effectively averages several maximum-amplitude observations.

Local Magnitude (M_L) Calculation

In keeping with common seismological practice, we compute the Richter magnitude for most events. Richter's scale relied on the then-widespread operation of a particular seismometer in southern California, known as the Wood–Anderson (WA) seismometer. Thus, for each seismograph, we deconvolve the modern instrument response and convolve a WA response to simulate the WA amplitude measurement. We utilize a 2080 sensitivity and damping constant of 0.7, rather than the previously widely reported sensitivity of 2800 and damping constant of 0.8 (Uhrhammer and Collins, 1990). For each horizontal component, we compute one-half the peak-to-trough amplitude, A, on the WA simulated displacement (in millimeters). Amplitudes are measured, automatically, within a 25 s window from the P-wave pick. During event review, an analyst will manually select a window corresponding to the maximum and minimum values of the S arrival for each horizontal component. Amplitudes are measured for each horizontal component at a station and then averaged for the station magnitude estimate.

As is commonly done in regional networks we formulate an amplitude distance-correction so that magnitude may be determined at each station within the network where:

$$M_L = \log A - \log A_0(x),$$

in which x is the distance (km) from the epicenter. The final event magnitude is the median of all station magnitudes within 10–160 km epicentral distance. We choose a minimum of 10 km epicentral distance because at close epicentral distances, and within the WA synthetic pass-band, there may be source-radiated energy in the spectrum above the Nyquist frequency. Thus, the maximum trace amplitudes that are used to calculate

Table 1
Significant Oklahoma Earthquakes

Date (yyyy/mm/dd)	Name	Magnitude	County
2016/09/03	Pawnee earthquake	5.8	Pawnee
2011/11/06	Prague earthquake	5.7	Lincoln
1952/04/09	El Reno earthquake	5.5	Canadian
2016/02/13	Fairview earthquake	5.1	Woods
2016/11/07	Cushing earthquake	5.0	Payne
1882/10/22	Choctaw Nation earthquake	4.8	Southeast Oklahoma
2011/11/05	Prague foreshock	4.8	Lincoln
2016/01/07	Fairview foreshock	4.8	Woods
2011/11/08	Prague aftershock	4.8	Lincoln
2015/11/19	Alfalfa County earthquake	4.7	Alfalfa

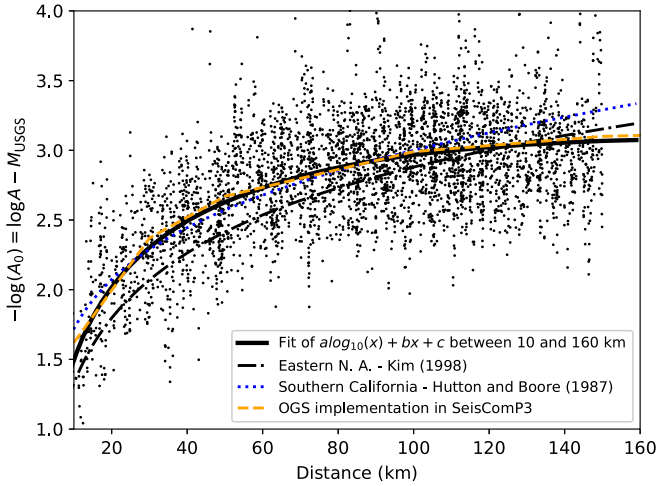

▲ **Figure 6.** log A_0 values for earthquakes that included USGS-recorded magnitude were derived using a moment tensor solution (M_{wr} or M_{ww}). The log A_0 term derives from the Richter equation described in the Local Magnitude (M_L) Calculation section and is used for calculating local magnitudes for smaller earthquakes. The color version of this figure is available only in the electronic edition.

the station M_L could be underestimated. We choose 160 km as the maximum window because this corresponds to the epicentral distance at which the P_n head wave traveling along the uppermost mantle would arrive at a station before the direct P wave (see Appendix). Local magnitude should be determined from direct body waves (Hutton and Boore, 1987), and so we do not consider more distant estimates of earthquake magnitude where the first P arrival would have traveled as a head wave along the crust–mantle interface.

We determined the fit to the previous equation using amplitudes from local network stations for earthquakes with a corresponding USGS-determined W-phase moment magnitude (M_{ww}) or regional moment tensor magnitude (M_{wr}). Because that magnitude is predetermined, we used the magnitude in the previous equation and computed values for the $-\log A_0$ value, which should be common to earthquakes of all magnitudes. We fit an equation of the form $a\log 10(x) + bx + c$ to the scatter of $-\log A_0$ values and determined coefficients: $a = 2.01$, $b = -0.0057$, and $c = -0.45$. In SC3, the function is replaced by a table of values, in which epicentral distances between points are interpolated between table entries. The function (black line) and interpolated table values (orange dashed line), as implemented in SC3, are shown in Figure 6. It should be noted that this M_L function differs from one previously used at OGS up until late 2018 (Darold *et al.*, 2014).

Within the WA synthetic response, earthquakes in the region produce surface waves with relatively larger amplitude than the S wave. When the peak amplitude is derived from a larger window that is larger than the first few seconds after S arrival, then the subsequent magnitude is relatively higher than the magnitude based on analyst-selected body-wave amplitudes. Therefore, there can be a difference between automatic (USGS M_L and OGS-automatic) and analyst-derived M_L. We typically find that this corresponds to an initial underestimation of event magnitude of ~0.1 to 0.2 magnitude units observed in both NEIC-reported M_L and automatic-M_L OGS reports. We analyzed 36 common events in 2019 for an area west of Oklahoma City and Norman and found that event magnitudes were 0.1 magnitude units lower than either the USGS M_L (0.1 median lower) or m_{bLg} magnitudes (0.1 median lower). We note that the systematic difference between OGS and USGS M_L values stems from a difference between using analyst-selected windows around the S wave (OGS) and automatic windows where the largest amplitude is used within the coda (USGS procedure for M_L).

EARTHQUAKE HAZARD AND RISK

The USGS updates the long-term National Seismic Hazard Map approximately every 6 yr. With the aforementioned increase in seismicity associated with unconventional resource plays in the past decade, the USGS sought to identify the short-term hazard in areas across the central United States and released short-term seismic hazard updates for 2016, 2017, and 2018 (Petersen *et al.*, 2016, 2017, 2018). Those updates followed the same methodology as the long-term model (Petersen *et al.*, 2014) including declustering earthquake catalogs so that the earthquake behavior approaches a Poissonian process whereby random, independent events (earthquakes) occur at a specific activity rate. Assuming the underlying rate of occurrence and the notion that there is a power-law distribution for occurrence of earthquake sizes (Gutenberg–Richter law), then one is able to estimate the underlying seismic hazard (Rosson *et al.*, 2019).

For the short-term hazard updates, USGS utilized earthquake occurrences within a short time period (2 yr with the most recent year weighted more heavily) to forecast the seismic hazard into the next year. In the most recent forecast for 2018, Petersen *et al.* (2018) forecasted a 10%–14% chance of moderate damage for an area adjacent to the Oklahoma City metro area and encompassing a broad swath of north-central Oklahoma. This represents a hazard nearly equivalent to some areas of California (Petersen *et al.*, 2014). It is unclear whether USGS will continue to update the short-term hazard model as a USGS spokesman is cited in a 8 July 2019 Tulsa World article (Associated Press, 2019): "The reason is because that induced seismicity has been decreasing every year since we did our first forecast back in 2015–2016, and as such, we're moving on to different priorities."

The state of Oklahoma is home to approximately four million people. Metropolitan areas of Oklahoma City and Tulsa are most vulnerable to the earthquake risk due to the larger number of structures and built environment. Because the seismic risk to the built environment is associated with the degree of shaking experienced during an earthquake, the OGS has identified soils statewide that may be susceptible to stronger shaking relative to other areas (Pritchett *et al.*, 2017). In that study, we categorized areas across the state

according to National Earthquake Hazard Reduction Program soil liquefaction classification scheme and found that both major metropolitan zones (Oklahoma City and Tulsa) may be more susceptible to stronger shaking and subsequent damage due to their proximity to the North Canadian and Arkansas Rivers, respectively. Further urban mapping would be required to better understand the soil structures that would be susceptible to strong shaking or liquefaction effects.

Most of the induced earthquakes have occurred on previously unmapped faults (Skoumal *et al.*, 2019), highlighting the difficulty of predicting earthquake hazard from induced seismicity. Many of these faults do not have sufficient displacement to be detectable with active-source seismic imaging. In early 2015, the Oklahoma Corporation Commission (OCC) issued a directive to limit wastewater injection to depths above the crystalline basement by "plugging-back" wells that extend into the basement. This was supposed to reduce the pore-pressure communication between the Arbuckle Group and the basement. However, many basement faults extend into the Arbuckle Group enabling pore-pressure migration into the basement. By mid-2015, the OCC put in a plan to reduce the daily injection rates and volumes in selected areas of interest (AOIs) with increased seismicity rate. This was complemented by a downturn of oil prices that forced reduction of production in regions deemed uneconomical for production.

In early 2016, the OCC took further measures by implementing daily reporting of injection data into the Arbuckle Group, an improvement to the monthly summary reports that are filed annually (OCC, 2015). Timely reporting of the more refined data provides the opportunity to more effectively mitigate seismic hazard on time, especially in response to large earthquakes; on numerous occasions the OCC would rapidly shut-in (halt disposal operations) or modify permits for reduced disposal in wells near larger (**M** 4.0+) events. A recent study suggests that some of these "rapid-response" actions were effective in reducing the rate of aftershocks following several large events, including the Pawnee and Cushing earthquakes (Goebel *et al.*, 2019).

Starting December 2016, the OCC designated the SCOOP/STACK region as an AOI and proactively implemented a stoplight protocol (OCC, 2016b) to mitigate hydraulic fracturing–triggered seismicity (Holland, 2013; Skoumal *et al.*, 2018). This protocol relies on the timely OGS catalog of earthquake epicenters and magnitudes to quickly determine the prescribed mitigating measures. As the earthquakes within wastewater injection AOI have declined, hydraulic fracturing in the SCOOP/STACK region has contributed almost half of the seismicity in Oklahoma in 2019. Thus, effective management and mitigation of earthquake risk continues to depend on effective monitoring by the OGS RSN.

CONCLUSIONS

As we outlined in prior sections, the OGS has been dedicated to understanding earthquake hazards for the past several decades. We summarized some of those more recent efforts and described the current regional seismic network that is part of ANSS. Earthquakes occur along the myriad faults across the state, whether or not that fault slip was promoted by wastewater injection. Starting around 2009, the rate of **M** 3.0+ earthquakes rose from about 2 or 3 per year to 579 and 903 in 2014 and 2015, respectively. Although that rate has since declined to pre-2014 rates, the seismic hazard in Oklahoma remains elevated relative to its tectonic background.

We have, in an ad-hoc fashion since 2010, built the infrastructure for a seismic network capable of robustly detecting seismicity, with near-real-time seismic processing and dissemination of information to the public. Our research into induced seismicity has provided the OCC with the technical guidance to more safely and effectively mitigate earthquake hazards. Furthermore, our work includes significant outreach and education of the populace regarding earthquake hazards. All these past, present, and future efforts should reduce the seismic risk for loss of property and life. Because Oklahoma does not have a substantial history of earthquakes, much work remains.

DATA AND RESOURCES

Waveform data recorded by OGS is available in real time at the Incorporated Research Institutions for Seismology (IRIS) Data Management Center at ds.iris.edu under Federated Digital Seismic Network codes OK (OGS; doi: 10.7914/SN/OK), O2 (OGS 2018+; doi: 10.7914/SN/02), Y7 (OGS/OU 2016–2019; doi: 10.7914/SN/Y7_2016), Y9 (OGS/OU 2016–2019; doi: 10.7914/SN/Y9_2016), and ZP (OGS 2016–2019; doi: 10.7914/SN/ZP_2016). The U.S. Geological Survey M_L values and amplitudes used for comparison were accessed through the Advanced National Seismic System's Comprehensive Catalog (https://earthquake.usgs.gov/data/comcat/). The OGS earthquake map is updated in real time (https://ogsweb.ou.edu/quake_viewer/), and the catalog can be downloaded for specific time periods and magnitude ranges (https://ogsweb.ou.edu/eq_catalog/). Some of the custom listener scripts and other utilities for the SeisComP3 system that were developed by OGS are available through public repositories (https://github.com/jakewalter/seiscomp_tools) or available by contacting the authors. The IRIS Mustang data quality can be accessed at http://services.iris.edu/mustang/. All websites were last accessed September 2019. The Ⓔ supplemental material includes a figure with the same information shown in Figure 3, though with station labels, and a table with sensor type for all stations operated by Oklahoma Geological Survey (OGS).

ACKNOWLEDGMENTS

The authors thank two anonymous reviewers and internal reviewers Peter Dotray, Brian Young, and Christian Poppeliers, whose comments improved the article. The authors acknowledge funding from the state of Oklahoma through Oklahoma Geological Survey (OGS) core funding as well as

supplementary funding through the Oklahoma Secretary for Energy and the Environment. The authors thank the analysts and other staff at OGS over the years who assisted in the earthquake monitoring efforts. Finally, the authors thank Oklahoma landowners for allowing them access to their properties to install seismographs. Some of the seismic instruments were provided by the Incorporated Research Institutions for Seismology (IRIS) through the Portable Array Seismic Studies of the Continental Lithosphere Instrument Center at New Mexico Tech. As stated previously, data collected will be available through the IRIS Data Management Center. The facilities of the IRIS Consortium are supported by the National Science Foundation under Cooperative Agreement Number EAR-1261681 and the Department of Energy (DOE) National Nuclear Security Administration. Sandia National Laboratories is a multimission laboratory managed and operated by National Technology and Engineering Solutions of Sandia, a limited liability company and a wholly owned subsidiary of Honeywell International, Inc., for the U.S. Department of Energy's National Nuclear Security Administration under Contract Number DE-NA0003525. This article describes objective technical results and analysis. Any subjective views or opinions that might be expressed in the article do not necessarily represent the views of the U.S. Department of Energy or the U.S. Government.

REFERENCES

Anthony, R. E., A. T. Ringler, D. C. Wilson, and E. Wolin (2018). Do low-cost seismographs perform well enough for your network? An overview of laboratory tests and field observations of the OSOP Raspberry Shake 4D, *Seismol. Res. Lett.* **90,** no. 1, 219–228, doi: 10.1785/0220180251.

Associated Press (2019). *Number of Oklahoma Earthquakes Drops for 4th Straight Year, Tulsa World, July 8, 2019*, https://www.apnews.com/2f9be17d9b1240aabd396de890723830 (last accessed August 2019).

Baker, E. M., and A. A. Holland (2013). *Probabilistic Seismic Hazard Assessment of the Meers Fault, Southwestern Oklahoma: Modeling and Uncertainties*, OGS Special Publication 2013–02.

Brudzinski, M. R., and M. Kozlowska (2019). Seismicity induced by hydraulic fracturing and wastewater disposal in the Appalachian Basin, USA: A review, *Acta Geophys.* **67,** no. 1, 351–364.

Chen, C., and A. A. Holland (2016). PhasePApy: A robust pure Python package for automatic identification of seismic phases, *Seismol. Res. Lett.* **87,** no. 6, doi: 10.1785/0220160019.

Chen, X., C. Pennington, J. Haffener, J. C. Chang, X. He, Z. Zhan, S. Ni, and J. I. Walter (2017). The Pawnee earthquake as a result of the interplay among injection, faults and foreshocks, *Scientif. Rep.* **7,** 4945, doi: 10.1038/s41598-017-04992-z.

Crone, A. J., and K. V. Luza (1990). Style and timing of Holocene surface faulting on the Meers fault, southwestern Oklahoma, *Geol. Soc. Am. Bull.* **102,** 1–17.

Darold, A., A. A. Holland, C. Chen, and A. Youngblood (2014). Preliminary analysis of seismicity near Eagleton 1–29, Carter County, *Oklahoma Geol. Surv. Open-File Rept. OF2-2014.*

Dudek, J. E. (2014). Understanding the Geologic Structure and Kinematics of the Keokuk Fault Zone in East-Central Oklahoma, *M.S. Thesis*, University of Tulsa.

Dycus, M. N. (2013). Structural Characterization of the Wilzetta Fault Zone; Lincoln, Pottawatomie, and Creek Counties, Oklahoma, *M.S. Thesis*, University of Tulsa.

Ellsworth, W. L. (2013). Injection-induced earthquakes, *Science* **341,** no. 6142, 1225942

Goebel, T., Z. Rosson, E. E. Brodsky, and J. I. Walter (2019). Aftershock deficiency of induced earthquake sequences during rapid mitigation efforts in Oklahoma, *Earth Planet. Sci. Lett.* **522,** 135–143, doi: 10.1016/j.epsl.2019.06.036.

Goebel, T. H. W., J. I. Walter, K. Murray, and E. E. Brodsky (2017). Comment on "How will induced seismicity in Oklahoma respond to decreased saltwater injection rates?" by C. Langenbruch and M. D. Zoback, *Sci. Adv.* **3,** no. 8, doi: 10.1126/sciadv.1700441.

Havskov, J., and L. Ottermöller (1999). SeisAn earthquake analysis software, *Seismol. Res. Lett.* **70,** no. 5, 532–534, doi: 10.1785/gssrl.70.5.532.

Holland, A. A. (2013). Earthquakes triggered by hydraulic fracturing in south-central Oklahoma, *Bull. Seismol. Soc. Am.* **103,** no. 3, 1784–1792, doi: 10.1785/0120120109.

Holland, A. A., K. Keranen, and E. Atekwana (2012). Preliminary results of the November 5, 2011, Mw5.6 earthquake sequence Prague, Oklahoma, *Assoc. Env. Eng. Geol. AEG News* **55,** no. 2, 15–16.

Hough, S. E., and M. Page (2015). A century of induced earthquakes in Oklahoma?, *Bull. Seismol. Soc. Am.* **105,** no. 6, 2863–2870.

Hutton, L. K., and D. M. Boore (1987). The M_L scale in southern California, *Bull. Seismol. Soc. Am.* **77,** no. 6, 2074–2094.

Keranen, K. M., H. M. Savage, G. A. Abers, and E. S. Cochran (2013). Potentially induced earthquakes in Oklahoma, USA: Links between wastewater injection and the 2011 Mw 5.7 earthquake sequence, *Geology* **41,** 699–702, doi: 10.1130/G34045.1.

Kim, W.-Y. (1998). The ML scale in eastern North America, *Bull. Seismol. Soc. Am.* **88,** 935–951.

Langenbruch, C., and M. D. Zoback (2016). How will induced seismicity in Oklahoma respond to decreased saltwater injection rates? *Sci. Adv.* **2,** no. 11, e1601542, doi: 10.1126/sciadv.1601542.

Lawson, J. E., and K. V. Luza (1995). Earthquake map of Oklahoma (with explanatory text), *Oklahoma Geol. Surv. Geologic Map 35*, scale 1:500,000.

Luza, K. V., and J. E. Lawson (1982). *Seismicity and Tectonic Relationships of the Nemaha Uplift in Oklahoma-Part IV*, OGS Special Publication 82–1.

Luza, K. V., R. F. Madole, and A. J. Crone (1987). *Investigation of the Meers Fault, Southwestern Oklahoma*, OGS Special Publication 87–1.

Mahani, A. B., and H. Kao (2018). Accurate determination of local magnitude for earthquakes in the Western Canada Sedimentary Basin, *Seismol. Res. Lett.* **90,** 203–211, doi: 10.1785/0220180264.

Marsh, S., and A. A. Holland (2016). Comprehensive fault database and interpretive fault map of Oklahoma, *Oklahoma Geol. Surv. Open-File Rept. OF2-2016*, 2 plates with supplement, 15 pp.

Murray, K. E., and A. A. Holland (2014). Inventory of Class II underground injection control volumes in the midcontinent, *Shale Shaker* **65,** no. 2, 98–106.

Northcutt, R. A., and J. A. Campbell (1995). Geological provinces of Oklahoma, *Oklahoma Geol. Surv. Open-File Rept. OF5–95.*

Oklahoma Corporation Commission (OCC) (2015). *Oil and Gas Disposal Well Volume Reduction Plan*, available athttp://www.occeweb.com/News/08-03-15VOLUME%20ADVISORY%20RELEASE.pdf, (last accessed August 2019).

OCC (2016a). *Regional Earthquake Response Plan for Central Oklahoma and Expansion of the Area of Interest*, available at http://www.occeweb.com/News/2016/03-07-16ADVISORY-AOI,%20VOLUME%20REDUCTION.pdf (last accessed August 2019).

OCC (2016b). *New Year, New Plays, New Plans*, available at http://www.occeweb.com/News/2016/12-20-16SCOOP-STACK.pdf (last accessed August 2019).

Petersen, M. D., M. P. Moschetti, P. M. Powers, C. S. Mueller, K. M. Haller, A. D. Frankel, Y. Zeng, S. Rezaeian, S. C. Harmsen, O. S. Boyd *et al.* (2014). Documentation for the 2014 update of the United States national seismic hazard maps, *U.S. Geol. Surv. Open-File Rept. 2014-1091*, 243 pp., doi: 10.3133/ofr20141091.

Petersen, M. D., C. S. Mueller, M. P. Moschetti, S. M. Hoover, A. L. Llenos, W. L. Ellsworth, A. J. Michael, J. L. Rubinstein, A. F. McGarr, K. S. Rukstale *et al.* (2016). 2016 one-year seismic hazard forecast for the Central and Eastern United States from induced and natural earthquakes. *U.S. Geol. Surv. Open-File Rept. 2016-1035*, 1–50, doi: 10.3133/OFR20161035.

Petersen, M. D., C. Mueller, M. P. Moschetti, S. M. Hoover, A. Shumway, D. E. McNamara, R. Williams, A. L. Llenos, W. L. Ellsworth, J. L. Rubinstein *et al.* (2017). 2017 one-year seismic hazard forecast for the central and eastern United States from induced and natural earthquakes, *Seismol. Res. Lett.* **88,** no. 3, 772–783, doi: 10.1785/0220170005.

Petersen, M. D., C. Mueller, M. P. Moschetti, S. M. Hoover, K. S. Rukstales, D. E. McNamara, R. A. Williams, A. Shumway, P. M. Powers, P. S. Earle *et al.* (2018). 2018 one-year seismic hazard forecast for the Central and Eastern United States from induced and natural earthquakes, *Seismol. Res. Lett.* **88,** doi: 10.1785/0220170005.

Pritchett, B. N., J. C. Chang, J. M. Chang, N. H. Suneson, and J. I. Walter (2017). Preliminary soil amplification map of Oklahoma according to the National Earthquake Hazard Reduction Program (NEHRP), *Oklahoma Geol. Surv. Geologic Map 41*, scale 1:500,000.

Regmi, N., and J. I. Walter (2019). Detailed mapping of shallow landslides in Eastern Oklahoma and potential triggering by Oklahoma earthquakes, *Geomorphology*, doi: 10.1016/j.geomorph.2019.05.026.

Rosson, Z., J. I. Walter, T. Goebel, and X. Chen (2019). Narrow spatial aftershock zones for induced earthquake sequences in Oklahoma, *Geophys. Res. Lett.* doi: 10.1029/2019GL083562.

Shah, A. K., and G. R. Keller (2017). Geologic influence on induced seismicity: Constraints from potential field data in Oklahoma, *Geophys. Res. Lett.* **44,** 152–161, doi: 10.1002/2016GL071808.

Skoumal, R. J., J. O. Kaven, and J. I. Walter (2019). Characterizing seismogenic fault structures in Oklahoma using a relocated template-matched catalog, *Seismol. Res. Lett.* **90,** doi: 10.1785/0220190045.

Skoumal, R. J., R. Ries, M. R. Brudzinski, A. J. Barbour, and B. S. Currie (2018). Earthquakes induced by hydraulic fracturing are pervasive in Oklahoma, *J. Geophys. Res.* **123,** doi: 10.1029/2018JB016790.

Stein, S., and M. Wysession (2003). *An Introduction to Seismology, Earthquakes, and Earth Structure*, Blackwell Publishing, Oxford, United Kingdom, 512 pp.

Stocker, M., J. Baffes, Y. Some, D. Vorisek, and C. Wheeler (2018). The 2014-16 Oil Price Collapse in Retrospect: Sources and Implications, *Policy Research Working Paper 8419*, World Bank, Washington, D.C.

Sumy, D. F., C. J. Neighbors, E. S. Cochran, and K. M. Keranen (2017). Low stress drops observed for aftershocks of the 2011 Mw5.7 Prague, Oklahoma, earthquake, *J. Geophys. Res.* **122,** 3813–3834, doi: 10.1002/2016JB013153.

Uhrhammer, R. A., and E. R. Collins (1990). Synthesis of Wood-Anderson seismograms from broadband digital records, *Bull. Seismol. Soc. Am.* **80,** 702–716.

Walsh, R. R., and M. D. Zoback (2015). Oklahoma's recent earthquakes and saltwater disposal, *Sci. Adv.* **1,** e1500195, doi: 10.1126/sciadv.1500195.

Walter, J. I., J. C. Chang, and P. J. Dotray (2017). Foreshock seismicity suggests gradual differential stress increase in the months prior to the 3 September 2016 Mw 5.8 Pawnee earthquake, *Seismol. Res. Lett.* **88,** no. 4, doi: 10.1785/0220170007.

Walter, J. I., C. Frohlich, and T. Borgfeldt (2018). Natural and induced earthquakes in the Texas and Oklahoma Panhandles, *Seismol. Res. Lett.* **89,** no. 6, 2437–2446, doi: 10.1785/0220180105.

Weber, B., J. Becker, W. Hanka, A. Heinloo, M. Hoffmann, T. Kraft, D. Pahlke, J. Reinhardt, J. Saul, and H. Thoms, (2007). SeisComP3–Automatic and interactive real time data processing, *Geophys. Res. Abstr. 9*, EGU General Assembly.

Weingarten, M., S. Ge, J. W. Godt, B. A. Bekins, and J. L. Rubinstein (2015). High-rate injection is associated with the increase in U.S. mid-continent seismicity, *Science* **348,** 1336–1340.

Yeck, W. L., G. P. Hayes, D. E. McNamara, J. L. Rubinstein, W. D. Barnhart, P. S. Earle, and H. M. Benz (2017). Oklahoma experiences largest earthquake during ongoing regional wastewater injection hazard mitigation efforts, *Geophys. Res. Lett.* **43,** doi: 10.1002/2016GL071685.

Yeck, W. L., M. Weingarten, H. M. Benz, D. E. McNamara, E. A. Bergman, R. B. Herrmann, J. L. Rubinstein, and P. S. Earle (2016). Far-field pressurization likely caused one of the largest injection induced earthquakes by reactivating a large preexisting basement fault structure, *Geophys. Res. Lett.* **43,** 10,198–10,207, doi: 10.1002/2016GL070861.

APPENDIX

CRITICAL DISTANCE FOR P_n PHASE

In Oklahoma, we analyzed the data to determine the critical distance for generation of a P_n phase, which is the P wave from an earthquake that travels as a head wave along the crust–mantle boundary. We plot the P-wave travel times with a reduced velocity corresponding to the mantle P-wave velocity (8.3 km/s). We estimate h_0, the thickness of the crust using the following equation (Stein and Wysession, 2003; Mahani and Kao, 2018):

$$h_0 = \tau/(2\sqrt{1/v_0^2 - 1/v_1^2}),$$

in which v_1 is the mantle velocity, v_0 is the reciprocal of the slope in Figure A1, and τ is the y-intercept or the head wave travel time at zero distance. Thus, the critical distance, x_c, below which the head wave is not present, can be calculated:

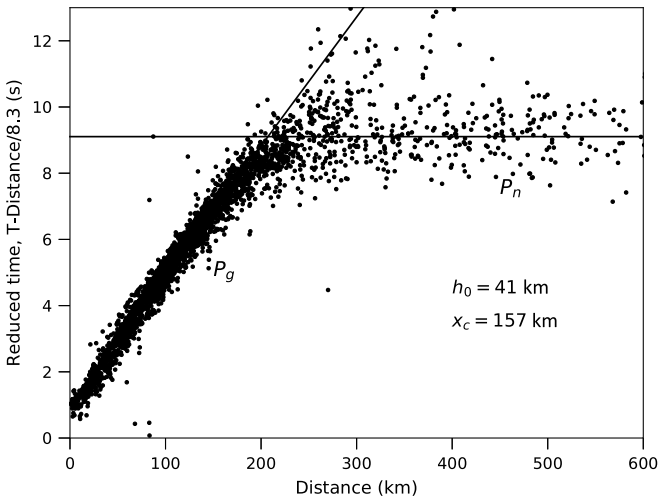

▲ **Figure A1.** Analyst-picked P-wave arrival time relative to event origin time.

$$x_c = 2h_0 \frac{v_0/v_1}{\sqrt{1-(v_0^2/v_1^2)}}.$$

We use these calculations to guide our earthquake processing where we do not utilize magnitude measurements that are greater than 160 km from the earthquake. This suggests that the crust is approximately 41 km thick, on average, and the distance at which P_n phases are present is approximately 160 km.

Jacob I. Walter
Paul Ogwari
Andrew Thiel
Fernando Ferrer
Isaac Woelfel
Oklahoma Geological Survey
University of Oklahoma
100 E. Boyd Street
Norman, Oklahoma 73019 U.S.A.
jwalter@ou.edu

Jefferson C. Chang
Hawaiian Volcano Observatory
U.S. Geological Survey
51 Crater Rim Drive
Hawai'i National Park
Hawaii, Hawaii 96718 U.S.A.

Amberlee P. Darold
Cascades Volcano Observatory
U.S. Geological Survey
1300 SE Cardinal Court Building 10
Vancouver, Washington 98683 U.S.A.

Austin A. Holland
Sandia National Laboratories
1515 Eubank Boulevard SE
Albuquerque, New Mexico 87123 U.S.A.

Published Online 13 November 2019